

# High-Flux Cold Ytterbium Atomic Beam Source Using Two-dimensional Laser Cooling with Intercombination Transition

Toshiyuki Hosoya<sup>1</sup>, Ryotaro Inoue<sup>2</sup>, Mikio Kozuma<sup>1,2</sup>

<sup>1</sup>Department of Physics, Tokyo Institute of Technology, 2-12-1 O-Okayama, Meguro-ku, Tokyo 152-8550, Japan

<sup>2</sup>Institute of Innovative Research, Tokyo Institute of Technology, 4259 Nagatsuta-cho, Midori-ku, Yokohama, Kanagawa 226-8503, Japan

We demonstrate a slow ytterbium atomic beam with a tunable longitudinal velocity in the range of 20–30 m/s, a transverse temperature of 11  $\mu$ K, and flux of up to  $1.2 \times 10^9$  atoms/s. Such performance is realized by applying two-dimensional cooling, with an intercombination transition, to a slow atomic beam generated by a dipolar-allowed transition. We also discuss the feasibility of narrowing the transverse momentum width to less than the recoil momentum using the velocity-selective optical transition of atoms based on a long-lived metastable state. Such a high-flux atomic beam will be a powerful tool for constructing compact and continuous Bragg diffraction interferometers with ytterbium atoms.

## 1. Introduction

Atom interferometry is a powerful tool for precision measurements [1],[2], that enables various inertial sensing applications such as gravity accelerometers [3][6], gravity gradiometers [7][12], and gyroscopes [13][19]. Since its inception, the field of interferometry with laser-cooled atoms has focused on alkali-metal atoms, which feature optical transitions favorable for laser cooling. Two-electron atoms, such as those in the alkaline-earth family or ytterbium (Yb), have been of particular interest for avoiding the influence of environmental magnetic fields. Further, gravity accelerometers [6] and gravity gradiometers [12] with laser-cooled two-electron atoms have also been realized using higher-order Bragg diffraction.

For gyroscopes with two-electron atoms, in addition to the pioneering work with thermal atomic beams [13], experiments using laser-cooled atoms to achieve higher accuracy have garnered attention. Simultaneously operated multiple atomic fountains [18] or laser-cooled slow atomic beams [19] are good candidates as laser-cooled atoms for interferometry. This is because practical applications require continuous data acquisition or a high data rate to avoid performance deterioration owing to dead time in atom interferometry. Although slow atomic beam generation has mainly been studied in the context of ultra-cold-atom-based experiments and optical lattice clock implementations [20][27], for Bragg-diffraction-based atom interferometry, the transverse momentum width of the atomic beam should be less than the recoil momentum of the Bragg beam [28]. Such an extreme narrowing of the momentum width has been realized by using a pair of slits for filtering out unwanted momentum

components from broad transverse momentum distributions in thermal atomic beam experiments [29]; however, this significantly reduces the beam flux.

In this study, we applied two-dimensional laser-cooling with an intercombination transition to a slow Yb atomic beam generated using a dipolar-allowed transition, resulting in the successful suppression of the transverse momentum width to the order of the recoil momentum of the Bragg beam while maintaining a beam flux of  $10^9$  atoms/s. Additionally, we have discussed the feasibility of further narrowing the momentum width by utilizing one of the long-lived metastable states of Yb.

The rest of this article is organized as follows. Section 2 describes the experimental setup and methods used to produce the atomic beam. We discuss the transverse temperature, longitudinal velocity, and atomic flux of the atomic beam after narrow-line cooling in Sec. 3. We elucidate the feasibility of further narrowing the momentum width by utilizing one of the long-lived metastable states of Yb in Sec. 4. Finally, we summarize our results in Sec. 5.

## 2. Experimental Setup

Figure 1 shows a schematic of our experimental setup. Our atomic beam is realized in three stages: slow atomic beam generation, beam deflection, and beam cooling based on narrow-line optical transition. In the first stage, a base slow atomic beam is generated by the Zeeman slowing of a thermal atomic beam from the oven, cooling and capturing of the decelerated atoms with a two-dimensional magneto-optical trap (2D-MOT), and

expelling of trapped atoms with a weak laser beam (pushing beam) [23].

The thermal atomic beam was produced using an effusive oven operating at 650 K, and the vacuum pressure in the 2D-MOT region is approximately  $10^{-7}$  Pa when the oven is operated. The magnetic field for the Zeeman slower (ZS) and the 2D-MOT was produced with four permanent magnets. The maximum magnetic field strength for the Zeeman slower was approximately 21 mT, and the magnetic field gradient for the 2D-MOT was 400 mT/m in the trapping area. The slow atomic beam is generated using the ZS beam, the 2D-MOT

We tested the deflector with  $\text{lin} \perp \text{lin}$  (2D-OM configuration [21]) and  $\sigma^+ - \sigma^-$  (2D-MOT configuration [22]) retroreflected beam polarizations. We evaluated the 2D-MOT configuration with a magnetic field gradient of 140 mT/m using a pair of permanent magnets [30]. However, it was found that the pointing of the atomic beam depended on the longitudinal velocity because the length of the 2D-MOT region is insufficient, and atoms acquire an offset transverse velocity depending on the incident longitudinal velocity. Thus, the 2D-OM configuration was adopted in the second stage.

In the third stage, the atomic beam is cooled to a lower transverse temperature using the  $^1\text{S}_0 - ^3\text{P}_1$  transition at a wavelength of 556 nm and a natural linewidth of  $\Gamma_{556}/2\pi = 182$  kHz, which corresponds to a Doppler temperature of 4.4  $\mu\text{K}$ , two orders of magnitude lower than the Doppler temperature of 690  $\mu\text{K}$  for the  $^1\text{S}_0 - ^1\text{P}_1$  transition. Generally, cooling parameters such as laser intensity, detuning, or magnetic field gradient are changed during narrow-line cooling to achieve both a wider capture range and a lower temperature [26][31][32]. Thus, we provided two narrow-line cooling regions to achieve both a wide capture range and a lower transverse temperature. The cooling beams in the first narrow-line cooling region exhibit greater detuning and stronger intensities than the beams in the second region to achieve a wider capture range. The cooling beam polarizations are in a 2D-OM configuration ( $\text{lin} \perp \text{lin}$ ). Each cooling beam in the first narrow-line region has a power of 45 mW, detuning of  $-7.9\Gamma_{556}$ , and a  $1/e^2$  diameter of 16 mm. The cooling beam in the second narrow-line cooling region has a near-resonant frequency and a weaker intensity than the beams in the first region to achieve lower transverse temperatures. Cooling beams in the second narrow-line region typically have a power of 3 mW, detuning of  $-3.7\Gamma_{556}$ , and a  $1/e^2$  diameter of 10 mm. The 556 nm cooling laser beam is generated by frequency-doubling a fiber laser output with a wavelength of 1112 nm and a linewidth of less than 20 kHz. The vacuum pressure in the narrow-line cooling region is less than  $10^{-8}$  Pa.

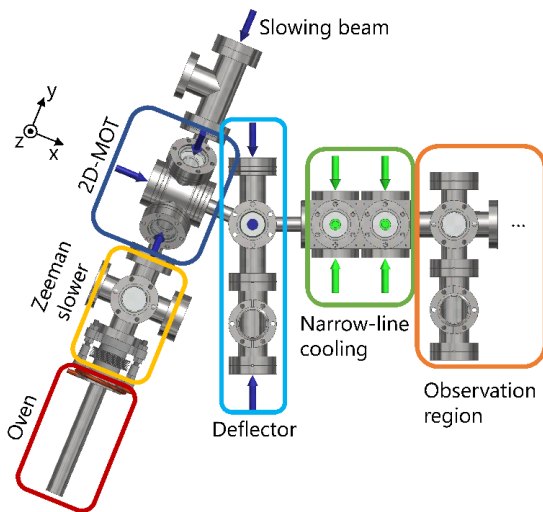


Figure 1: Schematic of the experimental setup. The atoms emitted from the effusive oven are decelerated by the Zeeman slower and are captured by the 2D-MOT. A weak laser beam expels trapped atoms from the 2D-MOT and generates the slow atomic beam. This slow beam is subsequently deflected via off-axis 2D-OM; particularly, it is radially cooled by two 2D-OM operating on the  $^1\text{S}_0 - ^3\text{P}_1$  transition (beams in green).

beams, and the pushing beam. Each beam is red-detuned from the  $^1\text{S}_0 - ^1\text{P}_1$  transition at a wavelength of 399 nm and a natural linewidth of  $\Gamma_{399}/2\pi = 29$  MHz. The ZS beam has a total power of 80 mW, detuning of  $-10\Gamma_{399}$ , and a  $1/e^2$  diameter of 7.8 mm, whereas the pushing beam has a total power of a few milliwatts, detuning of  $-1.7\Gamma_{399}$ , and a  $1/e^2$  diameter of 0.9 mm.

In the second stage, the base slow atomic beam is deflected by 22.5 degrees by the two-dimensional optical molasses (2D-OM) and is separated from the pushing beams. The vacuum pressure in the deflector region is less than  $10^{-8}$  Pa. The deflector beams have a power of 50 mW on the deflection plane axis and 5 mW on the orthogonal axis, a detuning from the  $^1\text{S}_0 - ^1\text{P}_1$  transition of  $-1\Gamma_{399}$ , and a  $1/e^2$  diameter of 9.7 mm.

### 3. Atomic Beam Properties

We first characterized the transverse temperature of the atomic beam after narrow-line cooling. The transverse temperature and longitudinal velocity of the atomic

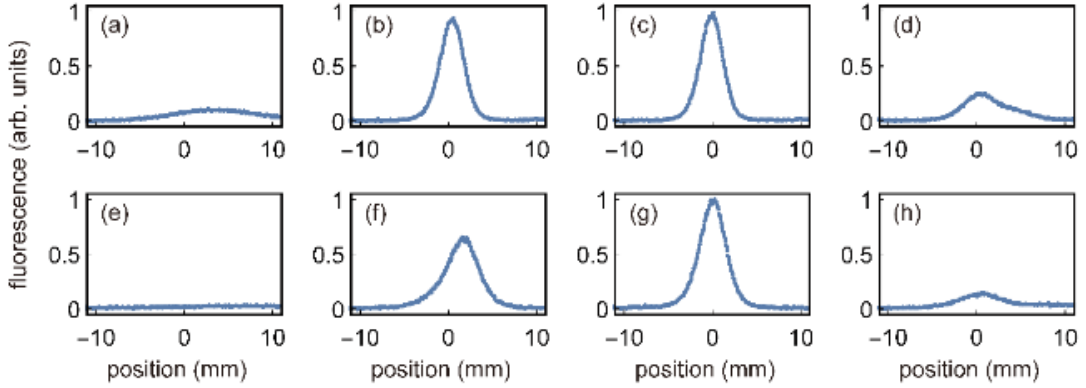


Figure 2: Effect of narrow-line cooling on atomic beam cross-section. Cross-sections were measured based on fluorescence imaging of the  $^1S_0$ – $^1P_1$  transition, with a CMOS camera placed (a) – (d) 260 mm and (e) – (h) 764 mm downstream of the second narrow-line cooling region. Atomic beam cross-sections measured (a), (e) without narrow-line cooling, (b), (f) with the first narrow-line cooling laser alone, (c), (g) with both the first and second narrow-line cooling lasers, and (d), (h) with the second narrow-line cooling laser alone. Fitting a Gaussian to the atomic beam cross-sections gives  $1/\sqrt{e}$  radii of (a)  $\sigma=5.1(3)$  mm, (b)  $\sigma=1.4(1)$  mm, (c)  $\sigma=1.3(1)$  mm, (e)  $\sigma=16(1)$  mm, (f)  $\sigma=2.0(1)$  mm, and (g)  $\sigma=1.5(1)$  mm.

beam before it enters the narrow-line cooling region are 1.6(1) mK and 30(1) m/s, respectively. The transverse temperature and longitudinal velocity are estimated through the Doppler shift and broadening in the fluorescence spectroscopy results of the  $^1S_0$ – $^3P_1$  transition.

Figure 2 shows cross-sections of four atomic beam patterns, generated without narrow-line cooling [Fig. 2 (a) and (e)], with the first narrow-line cooling laser alone [Fig. 2 (b) and (f)], with the first and second narrow-line cooling lasers [Fig. 2 (c) and (g)], and with the second narrow-line cooling laser alone [Fig. 2 (d) and (g)]. These cross-sections were measured 260 mm [Fig. 2 (a) – (d)] and 764 mm [Fig. 2 (e) – (h)] downstream of the second narrow-line cooling region through fluorescence imaging of the  $^1S_0$ – $^1P_1$  transition with a complementary metal-oxide-semiconductor (CMOS) camera. The atomic beam divergences become smaller as the number of narrow-line cooling regions increases; that is, the transverse temperatures decrease [Fig. 2 (a) – (c) and (e) – (g)]. However, the atomic fluxes are not significantly different. The cross-section produced with only the second narrow-line cooling laser has double distributions, and each distribution has a different divergence, suggesting that the transverse temperature also has a double distribution [Fig. 2 (d) and (h)]. The two narrow-line cooling regions are necessary to achieve both a wide capture range and lower transverse temperature in our system.

Figure 3 shows the dependence of the divergence angle on the second narrow-line cooling laser beam power and

detuning. The divergence angle,  $\theta_\sigma$ , is given as

$$\theta_\sigma = \arctan[(\sigma_{764mm} - \sigma_{260mm})/\Delta L],$$

where  $\sigma_{260mm}$  and  $\sigma_{764mm}$  are the  $1/\sqrt{e}$  radii evaluated by fitting a Gaussian to the atomic beam cross-section 260 mm and 764 mm downstream of the second narrow-line cooling region, respectively, and  $\Delta L$  is the distance between the two measurement points, 504 mm in this instance. The minimum  $\theta_\sigma$  for the second narrow-line cooling beams is 0.34(2) mrad, where the total power and detuning are 3 mW and  $-3.7\Gamma_{556}$ , respectively. In this case, a transverse temperature of 11(9)  $\mu\text{K}$  is estimated by measuring the expansion of the atomic beam size [33], which is lower than the 84(14)  $\mu\text{K}$  produced using only the first narrow-line cooling laser. This transverse

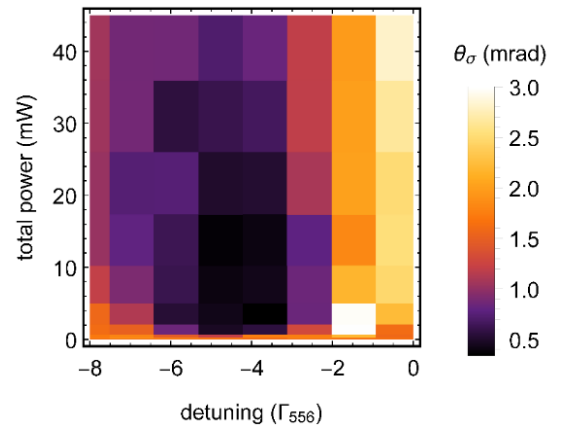


Figure 3: Atomic beam divergence as a function of the total cooling beam power and the detuning of the cooling beam in the second narrow-line cooling region.

temperature is close within errors to the Doppler temperature of  $14 \mu\text{K}$  calculated with the 2D-OM configuration with a detuning of  $-3.7\Gamma_{556}$  [34].

The longitudinal velocity of the atomic beam after narrow-line cooling can be controlled by changing the pushing beam power. The longitudinal velocity distribution is characterized using time-of-flight (TOF) measurements. A plug beam resonant on the  $^1\text{S}_0 - ^1\text{P}_1$  transition was used to block the atomic beam and was positioned 260 mm downstream of the second narrow-line cooling region. Atomic beam pulses were generated by turning off the plug beam for 0.5 ms. The temporal variation of the fluorescence was measured by a photomultiplier tube 764 mm downstream of the second narrow-line cooling region based on a probe beam resonant on the  $^1\text{S}_0 - ^1\text{P}_1$  transition. As shown in Fig. 4, the mean longitudinal velocity varied from 20 m/s to 30 m/s as the pushing beam power was increased from 1 mW to 3 mW. In this range, the transverse temperature is less than  $20 \mu\text{K}$ , and the total flux exceeds  $7 \times 10^8$  atoms/s.

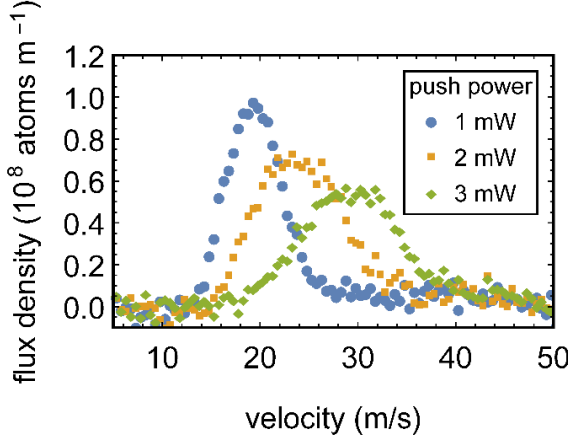


Figure 4: Longitudinal velocity distribution of the atomic beam, for pushing beam powers of 1, 2, and 3 mW.

As the scale factor of a Mach-Zehnder Bragg interferometer is inversely proportional to longitudinal velocity [14], we analyzed the stability of this parameter by measuring the mean longitudinal velocity at every 30 s for 3.2 h, using the TOF method. The results of these measurements are shown in Fig. 5. In our setup, the stability of the mean velocity is restricted by that of the pushing beam intensity and detuning; by contrast, the stability of the mean velocity is improved when using three-dimensional optical molasses [35].

Figure 6 (a) shows the dependence of the total flux on oven temperature. The total atomic flux was calculated

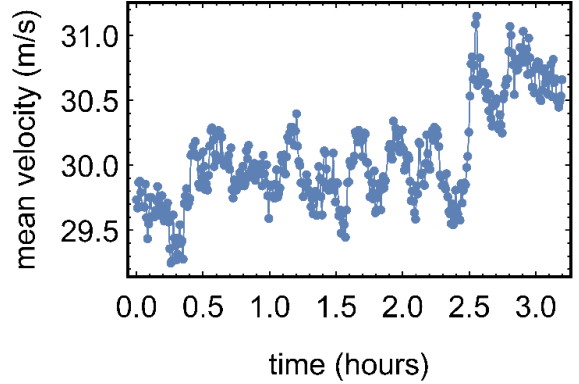


Figure 5: Mean longitudinal velocity with a pushing beam power of 3 mW as a function of time.

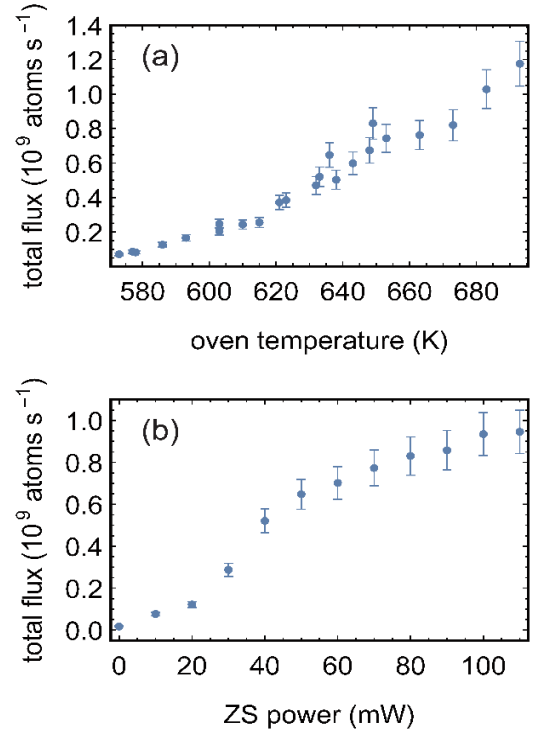


Figure 6: (a) Atomic flux with a pushing beam power of 2 mW as a function of oven temperature. (b) Atomic flux with a pushing beam power of 2 mW as a function of ZS power.

by integrating the flux density with respect to velocity from TOF measurements. The total flux increases monotonically with respect to oven temperature in the  $573 - 693 \text{ K}$  range. The maximum flux is  $1.2(2) \times 10^9$  atoms/s at 693 K. Here, the pushing beam power was 2 mW, and the parameters for narrow-line cooling were set to minimize the divergence angle  $\theta_\sigma$ . The total flux also depends on the ZS power, as shown in Fig. 6(b), and a ZS power of 80 mW was employed for the experiments described in Sec. 3.

#### 4. Momentum width filtering with ultra-narrow line transition

In higher-order Bragg interferometers, the transverse momentum width of the cold atomic beam must be less than the recoil momentum [28]. Herein, we propose a scheme to satisfy this requirement using an ultra-narrow line transition of ytterbium atoms. Note that one can reduce the momentum width by using simple mechanical slits [29], but the atoms will have to propagate by several meters to minimize the flux loss.

Ytterbium atoms have long-lived metastable states such as the  $^3P_0$  and  $^3P_2$  states. By irradiating such atoms with a laser pulse resonant on a transition between the ground and metastable states, one can transfer the atoms from one state to another in a momentum-selective manner, where the momentum width is determined by the interaction time, i.e., the transit time. Several methods can be considered to obtain a narrow momentum width for the cold atomic beam demonstrated in this study. One possibility is velocity-selectively exciting atoms to the metastable state, blowing away atoms in the ground state by a resonant light on the  $^1S_0$ – $^1P_1$  transition and then velocity-selectively returning the atoms to the ground state. Another method is pumping all atoms to the metastable state and velocity-selectively transferring atoms to the ground state. Herein, we present numerical results based

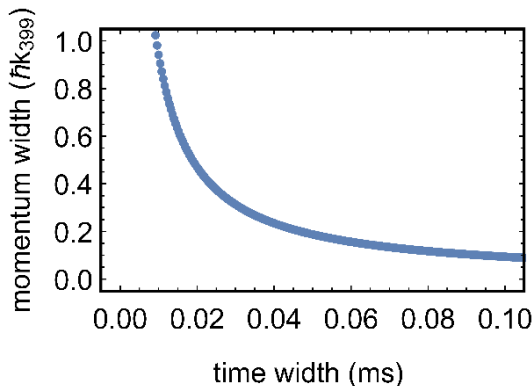


Figure 7: Numerical calculation of the momentum width of atoms as a function of the time width. The time width is the beam waist divided by longitudinal velocity of the atomic beam. Atoms are first excited to the  $^3P_2$  state by a  $\pi$ -pulse laser. Then, the ground state of the atoms is blown away, and the  $^3P_2$  state of atoms is transferred to the ground state again with a  $\pi$ -pulse laser.

on the former method using the ultra-narrow transition between the ground state and the  $^3P_2$  state, which has a lifetime of 15 s [36].

Figure 7 shows the results of the numerical calculation based on the optical Bloch equation, where the time width is given by the beam waist of laser light divided by the longitudinal atom velocity of 25 m/s. A momentum width of  $0.23\hbar k_{399}$  can be achieved using laser light with a beam waist of 1 mm and peak intensity of  $1.2\text{ kW/cm}^2$ <sup>1</sup>. Total power on the order of 10 W is necessary to perform the momentum selection, and such a high-power laser field can be prepared by using an optical cavity [38].

#### 5. Conclusions

We have demonstrated an ytterbium slow atomic beam with an ultra-low transverse temperature. The beam was generated using a three-stage setup consisting of a 2D-MOT, a deflector, and narrow-line cooling. The narrow-line cooling stage is divided into two regions, which are required for achieving a wide capture range and a lower transverse temperature. The two stages of narrow-line cooling successfully decrease the transverse temperature from  $1.6(1)$  mK to  $11(9)$   $\mu\text{K}$ . The mean longitudinal velocity varies from 20 m/s to 30 m/s upon increasing the pushing beam power from 1 mW to 3 mW, while the transverse temperature is maintained below 20  $\mu\text{K}$ , and the total flux is greater than  $7 \times 10^8$  atoms/s. An atomic flux of  $1.2(2) \times 10^9$  atoms/s was achieved with an oven temperature of 693 K. Furthermore, we have shown the feasibility of further narrowing the momentum width such that it is less than the recoil momentum by utilizing the  $^3P_2$  states of Yb. Such a high-flux slow atomic beam with a momentum width less than the recoil momentum can be useful for constructing compact and continuous Bragg diffraction interferometers with ytterbium atoms.

#### ACKNOWLEDGMENTS

This study was supported by the JST-MIRAI Program Grant No. JPMJMI17A3. T.H. acknowledges partial support from the Japan Society for the Promotion of Science.

<sup>1</sup> The Rabi frequency  $\Omega$  of the  $^1S_0$ – $^3P_2$  M2 transition for bosonic isotopes of Yb is given as  $\Omega/2\pi = 2.04\sqrt{I}$ , where  $I$

is the intensity of the excitation laser [37].

[1] L. Zhou, S. Long, B. Tang, X. Chen, F. Gao, W. Peng, W. Duan, J. Zhong, Z. Xiong, J. Wang, Y. Zhang, M. Zhan, Test of Equivalence Principle at  $10^{-8}$  Level by a Dual-Species Double-Diffraction Raman Atom Interferometer, *Phys. Rev. Lett.* 115 (2015) 013004.

[2] R. Bouchendira, P. Cladé, S. Guellati-Khélifa, F. Nez, F. Biraben, New Determination of the Fine Structure Constant and Test of the Quantum Electrodynamics, *Phys. Rev. Lett.* 106 (2011) 080801.

[3] M. Kasevich, S. Chu, Measurement of the gravitational acceleration of an atom with a light-pulse atom interferometer, *Appl. Phys. B Photophysics Laser Chem.* 54 (1992) 321–332.

[4] A. Peters, K.Y. Chung, S. Chu, Measurement of gravitational acceleration by dropping atoms, *Nature*. 400 (1999) 849–852.

[5] H. Müller, S. Chiow, S. Herrmann, S. Chu, K.-Y. Chung, Atom-Interferometry Tests of the Isotropy of Post-Newtonian Gravity, *Phys. Rev. Lett.* 100 (2008) 031101.

[6] T. Mazzoni, X. Zhang, R. Del Aguila, L. Salvi, N. Poli, G.M. Tino, Large-momentum-transfer Bragg interferometer with strontium atoms, *Phys. Rev. A*. 92 (2015) 053619.

[7] M. Snadden, J. McGuirk, P. Bouyer, K. Haritos, M. Kasevich, Measurement of the Earth's Gravity Gradient with an Atom Interferometer-Based Gravity Gradiometer, *Phys. Rev. Lett.* 81 (1998) 971–974.

[8] J.M. McGuirk, G.T. Foster, J.B. Fixler, M.J. Snadden, M.A. Kasevich, Sensitive absolute-gravity gradiometry using atom interferometry, *Phys. Rev. A*. 65 (2002) 033608.

[9] A. Bertoldi, G. Lamporesi, L. Cacciapuoti, M. de Angelis, M. Fattori, T. Petelski, A. Peters, M. Prevedelli, J. Stuhler, G.M. Tino, Atom interferometry gravity-gradiometer for the determination of the Newtonian gravitational constant G, *Eur. Phys. J. D*. 40 (2006) 271–279.

[10] F. Sorrentino, Q. Bodart, L. Cacciapuoti, Y.-H. Lien, M. Prevedelli, G. Rosi, L. Salvi, G.M. Tino, Sensitivity limits of a Raman atom interferometer as a gravity gradiometer, *Phys. Rev. A*. 89 (2014) 023607.

[11] G. D'Amico, F. Borselli, L. Cacciapuoti, M. Prevedelli, G. Rosi, F. Sorrentino, G.M. Tino, Bragg interferometer for gravity gradient measurements, *Phys. Rev. A*. 93 (2016) 063628.

[12] R.P. del Aguila, T. Mazzoni, L. Hu, L. Salvi, G.M. Tino, N. Poli, Bragg gravity-gradiometer using the  $^1S_0 - ^3P_1$  intercombination transition of  $^{88}\text{Sr}$ , *New J. Phys.* 20 (2018) 043002.

[13] F. Riehle, T. Kisters, A. Witte, J. Helmcke, C.J. Bordé, Optical Ramsey spectroscopy in a rotating frame: Sagnac effect in a matter-wave interferometer, *Phys. Rev. Lett.* 67 (1991) 177–180.

[14] T.L. Gustavson, P. Bouyer, M.A. Kasevich, Precision Rotation Measurements with an Atom Interferometer Gyroscope, *Phys. Rev. Lett.* 78 (1997) 2046–2049.

[15] T.L. Gustavson, A. Landragin, M.A. Kasevich, Rotation sensing with a dual atom-interferometer Sagnac gyroscope, *Class. Quantum Gravity*. 17 (2000) 2385–2398.

[16] B. Canuel, F. Leduc, D. Holleville, A. Gauguet, J. Fils, A. Virdis, A. Clairon, N. Dimarcq, C.J. Bordé, A. Landragin, P. Bouyer, Six-Axis Inertial Sensor Using Cold-Atom Interferometry, *Phys. Rev. Lett.* 97 (2006) 010402.

[17] A. Gauguet, B. Canuel, T. Lévèque, W. Chaibi, A. Landragin, Characterization and limits of a cold-atom Sagnac interferometer, *Phys. Rev. A*. 80 (2009) 063604.

[18] D. Savoie, M. Altorio, B. Fang, L.A. Sidorenkov, R. Geiger, A. Landragin, Interleaved atom interferometry for high-sensitivity inertial measurements, *Sci. Adv.* 4 (2018) eaau7948.

[19] H. Xue, Y. Feng, S. Chen, X. Wang, X. Yan, Z. Jiang, Z. Zhou, A continuous cold atomic beam interferometer, *J. Appl. Phys.* 117 (2015) 094901.

[20] A. Witte, T. Kisters, F. Riehle, J. Helmcke, Laser cooling and deflection of a calcium atomic beam, *J. Opt. Soc. Am. B*. 9 (1992) 1030.

[21] U. Dammalapati, I. Norris, L. Maguire, M. Borkowski, E. Riis, A compact magneto-optical trap apparatus for calcium, *Meas. Sci. Technol.* 20 (2009) 095303.

[22] T. Yang, K. Pandey, M.S. Pramod, F. Leroux, C.C. Kwong, E. Hajiyev, Z.Y. Chia, B. Fang, D. Wilkowski, A high flux source of cold strontium atoms, *Eur. Phys. J. D*. 69 (2015) 226.

[23] I. Nosske, L. Couturier, F. Hu, C. Tan, C. Qiao, J. Blume, Y.H. Jiang, P. Chen, M. Weidmüller, Two-dimensional magneto-optical trap as a source for cold strontium atoms, *Phys. Rev. A*. 96 (2017) 053415.

[24] M. Barbiero, M.G. Tarallo, D. Calonico, F. Levi, G. Lamporesi, G. Ferrari, Sideband-Enhanced Cold Atomic Source for Optical Clocks, *Phys. Rev. Appl.* 13 (2020) 014013.

[25] C.-C. Chen, S. Bennetts, R.G. Escudero, B. Pasquiou, F. Schreck, Continuous Guided Strontium Beam with High Phase-Space Density, *Phys. Rev. Appl.* 12 (2019) 044014.

[26] S. Dörscher, A. Thobe, B. Hundt, A. Kochanke, R. Le Targat, P. Windpassinger, C. Becker, K. Sengstock, Creation of quantum-degenerate gases of ytterbium in a compact 2D-/3D-magneto-optical trap setup, *Rev. Sci. Instrum.* 84 (2013) 043109.

[27] E. Wodey, R.J. Rengelink, C. Meiners, E.M. Rasel, D. Schlippert, A robust, high-flux source of laser-cooled ytterbium atoms, *J. Phys. B At. Mol. Opt. Phys.* 54 (2021) 035301.

[28] S.S. Szigeti, J.E. Debs, J.J. Hope, N.P. Robins, J.D. Close, Why momentum width matters for atom interferometry with Bragg pulses, *New J. Phys.* 14 (2012) 023009.

[29] D.M. Giltner, R.W. McGowan, S.A. Lee, Atom Interferometer Based on Bragg Scattering from Standing Light Waves, *Phys. Rev. Lett.* 75 (1995) 2638–2641.

- [30] T.G. Tiecke, S.D. Gensemer, A. Ludewig, J.T.M. Walraven, High-flux two-dimensional magneto-optical-trap source for cold lithium atoms, *Phys. Rev. A.* 80 (2009) 013409.
- [31] F. Riehle, T. Kisters, A. Witte, J. Helmcke, C.J. Bordé, Optical Ramsey spectroscopy in a rotating frame: Sagnac effect in a matter-wave interferometer, *Phys. Rev. Lett.* 67 (1991) 177–180.
- [32] S.L. Kemp, K.L. Butler, R. Freytag, S.A. Hopkins, E.A. Hinds, M.R. Tarbutt, S.L. Cornish, Production and characterization of a dual species magneto-optical trap of cesium and ytterbium, *Rev. Sci. Instrum.* 87 (2016) 023105.
- [33] H. Chen, E. Riis, Cold atomic beam from a rubidium funnel, *Appl. Phys. B.* 70 (2000) 665–670.
- [34] N.D. Gomes, M.A. Caracanhas, K.M. Farias, V.S. Bagnato, Laser cooling techniques: standard and alternated optical molasses, *Rev. Bras. Ensino Física.* 39 (2017).
- [35] J.M. Kwolek, C.T. Fancher, M. Bashkansky, A.T. Black, Three-Dimensional Cooling of an Atom-Beam Source for High-Contrast Atom Interferometry, *Phys. Rev. Appl.* 13 (2020) 044057.
- [36] S.G. Porsev, Y.G. Rakhлина, M.G. Kozlov, Electric-dipole amplitudes, lifetimes, and polarizabilities of the low-lying levels of atomic ytterbium, *Phys. Rev. A - At. Mol. Opt. Phys.* 60 (1999) 2781–2785.
- [37] A. Yamaguchi, Metastable State of Ultracold and Quantum Degenerate Ytterbium Atoms: High-Resolution Spectroscopy and Cold Collisions, Kyoto University, 2008.
- [38] X.-H. Bao, A. Reingruber, P. Dietrich, J. Rui, A. Dück, T. Strassel, L. Li, N.-L. Liu, B. Zhao, J.-W. Pan, Efficient and long-lived quantum memory with cold atoms inside a ring cavity, *Nat. Phys.* 8 (2012) 517–521.